Silicon (2023) 15:61–70
https://doi.org/10.1007/s12633-022-01962-7

ORIGINAL PAPER

Insight on the Dependence of the Drug Delivery Applications of Mesoporous Silica Nanoparticles on Their Physical Properties

Mohamed M. Fathy[1] · Fatma M. Yassin[1] · Wael M. Elshemey[2] · Heba M. Fahmy[1]

Received: 21 February 2022 / Accepted: 10 June 2022 / Published online: 4 July 2022

Abstract

Summary Mesoporous silica nanoparticles (MSNs) are fascinating due to their interesting properties and applications.

Purpose The optimization of MSNs for drug delivery applications was achieved by preparing different formulations of MSNs using different concentrations of ammonium hydroxide (NH_4OH) (0.7, 1.4, 2.8, 4.2, and 5.6 mg/ml for MSN1, MSN2, MSN3, MSN4, and MSN5, respectively).

Methods In the synthesis of MSNs, NH_4OH was used as a catalyst while tetraethyl orthosilicate were used as a source of silica. Transmission electron microscopy (TEM) image revealed a linear increase in the size of the formed MSNs with increase in catalyst concentration. TEM images showed that all investigated nanoparticles were dispersed and spherical (changed to oval on addition of higher concentration of NH_4OH).

Results The hydrodynamic sizes of prepared MSNs were (64.18 ± 6.8, 90.46 ± 7.1, 118.98 ± 7.01, 152.7 ± 1.7, and 173.9 ± 9.36 nm for MSN1, MSN2, MSN3, MSN4, and MSN5, respectively) assessed using the dynamic light scattering (DLS) technique. The negative values of zeta potential indicated high surface stability of the formed MSNs. N_2-isotherm revealed that the pore volume of MSNs decreased with increase in the size of MSNs. In vitro drug release showed that all MSNs exhibited high encapsulation efficiency of doxorubicin. The encapsulation efficiency were 92.2%, 82.8%, 72.2%, 72.1% and 71.9%for MSN1, MSN2, MSN3, MSN4, and MSN5, respectively.

Conclusion MSN1 and MSN2, with sizes of 64.18 ± 6.8 and 90.46 ± 7.1 nm, pore volume of 0.89 and 0.356 cc/g, encapsulation efficiency of 92.2% and 82.8%, and adequate drug release profiles, were probably the best choices for a drug carrier in drug delivery applications.

Keywords Mesoporous silica nanoparticles · Nano-catalyst · Doxorubicin · Drug delivery

1 Introduction

Nanoparticles attracted incredible interest due to the gap between bulk materials and atomic or sub-atomic structures. Particles at the nanoscale have different chemical, physical, optical and mechanical properties. So, they have vastapplications in drug delivery as nano-drug carriers.Among these are,eliminating drug overdose, increasing solubility, decreasing immunogenicity, reducing side effects, providingspecific reach of the drug to the target cell [1],and beating the pharmacokinetics impediments [2]. This provides advantages that help treat diseases that were previously difficult to treat [3].

Mesoporous silica nanoparticles (MSNs) are important for drug delivery applications [4]. MSNs are spherical nanoparticles consisting of several pores isolated from each other by a solid skeleton [5]. MSNs have distinguished properties, such as a large surface area, uniform and customizable pore size, and large pore volume [5–7]. These attractive features make MSNs applicable in many areas, including hyperthermia treatment, diagnostics,catalysis,adsorbents,antireflection coating,sensing, and drug delivery [8–16]. Based on these features, MSNs are the most important nanoparticles used as drug carriers in medicate delivery. The vital characteristic

This manuscript was written with contributions from all authors.

✉ Mohamed M. Fathy
mfathy@sci.cu.edu.eg

✉ Fatma M. Yassin

[1] Biophysics Department, Faculty of Science, Cairo University, 12613 Giza, Egypt

[2] Department of Physics, Faculty of Science, Islamic University of Madinah, Medina, Kingdom of Saudi Arabia

for enhancing drug delivery to a target cell is the size of MSNs. The cellular uptake of MSNs is affected by particle size, which affects the interaction of MSNs with the cell membrane [17–20]. The uptake by target cells increases as nanoparticles decrease [21]. The electrical, magnetic, optical, thermodynamic, and mechanical properties of nanomaterials are size-dependent; therefore, an accurate determination of the size of nanoparticles is essential [22, 23].

The most common method to synthesize MSNs is templating [24, 25]. It involves synthesizing MSNs using surfactants (pore producing agents) as templates, allowing the synthesis of MSNs with different morphologies, mesostructures, and dimensions by controlling the reaction conditions [26, 27]. Researchers have used various strategies to tailor the properties of MSNs with different textural properties. Some studies have used different templating agents to synthesize MSNs, producing MSNs with less than 4 nm [28–32]. Moreover, the effect of the presence and absence of hexanol, as a cosolvent in the reactant solution, on the morphology and mesostructure of MSNswas studied. With hexanol, the sizes of the particles become larger [33]. Some studies investigated the impact of not stirring [34, 35] or stirring many times [36, 37] on the MSN preparation. Other works studied the effect of xylene, toluene, and trimethylbenzene (TMB) (as different swelling operators), time and temperature of synthesis, different silica sources [tetraethyl orthosilicate (TEOS) versus tetramethylorthosilicate], and silica/surfactant ratio on the synthesis of MSNs [38, 39]. Nooney et al. [40] synthesized MSNs using different ratios of TEOS–surfactant under dilute conditions, and their results showed that the synthesized MSNs ranged from 65 to 740 nm. Vazquez et al. [41] examined the impact of distinct molar proportions of NH_3/TEOS, water/TEOS, and surfactant cetyltrimethyl-ammonium bromide (CTAB) on the morphology, pore size, and surface area of synthesized MSNs.

Different characterization techniques were used to estimate the different properties of the nanoparticles. These properties guide researchers to the possible use of nanoparticles in specific applications. Some of the previous studies combined different techniques to characterize nanoparticles, such as using small-angle X-ray scattering (SAXS) and wide-angle X-ray scattering (WAXS) in the study of oxide-supported platinum nanoparticle solution [42]. Using SAXS, TEM, and DLS in the characterization of shell crosslinked nanoparticles [43],surface-functionalized gold nanoparticles [44], and the formation of silica nanoparticles in different suspensions [45, 46] are all reported. Moreover, Sponchiaet al. used different characterization techniques, SAXS, BET, X-ray powder diffraction (XRD), and TEM, to characterize the pore size of MSNs [7]. Pabischet al. combined SAXS, DLS, Brunauer–Emmett–Teller (BET), XRD, and TEM to characterize oxide nanoparticles [47].

This study focuses on preparing and characterizing several MSN formulations using different concentrations of ammonium hydroxide (NH4OH) as a catalyst and studying their applicability in the in vitro delivery of anticancer drug doxorubicin (DOX). The characterization is performed using different biophysical techniques: TEM, DLS, SAXS, WAXS, gas isotherm (N_2-isotherm), and atomic force microscopy (AFM).

Although most of the previous research were focused on using various strategies for tailoring the properties of MSNs with different textural properties, there is still a lack of reports discussing, in depth, the effect of internal properties of nanoparticles on drug encapsulation and release. This work aimed at fulfilling this gap through employment of various characterization techniques providing deep insight on the structural properties of the investigated MSNs and their relation to drug encapsulation and release. The control of these parameters would significantly promote the usage of MSNs in drug delivery applications.

2 Experimental Section

2.1 Materials

Ammonium hydroxide NH_4OH (28%) was purchased from Fluka (USA). Doxorubicin hydrochloride (DOX) with concentration 2 mg/mL and ethanol alcohol (99%) were purchased from Sigma-Aldrich (St. Louis, MO, USA). 2-Ethoxyethanol LR (99%) was purchased from SDFCL company (India). Phosphate-buffered saline (PBS) pH 7.4 was purchased from Biodiagnostic Co. (Giza, Egypt). TEOS(99%) and cetyltrimethyl-ammonium bromide (CTAB, 99%) were purchased from Merck (Germany).

2.2 Preparation of MSNs

Mesoporous silica nanoparticles were synthesized according to Chen et al. [48]. CTAB (0.5 g) was dissolved in 70-ml deionized water, and then 0.7-mg/ml NH_4OH and 30-ml 2-ethoxyethanol (cosolvent) were added to the solution. After 30 min of stirring at room temperature, 2.5ml of TEOS was added. The white precipitate was collected and washed using ethyl alcohol and deionized water. To remove CTAB residuals, the sample was calcined at 600 °C for 6 h.

To study the impact of ammonia concentration on the physical characteristics of the prepared MSNs, different samples of MSNs were prepared using the same steps at different concentrations of NH_4OH: 0.7, 1.4, 2.8, 4.2, and 5.6 mg/ml. The samples were named MSN1, MSN2, MSN3, MSN4, and MSN5, respectively.

2.3 Characterization

The morphology and average size of MSNs were analyzed using transmission electron microscopy (TEM) (JEM

1230 electron microscope Jeol, Tokyo, Japan). The mean hydrodynamic diameter and the number of surface charges (zeta potential) were determined using the ZetasizerNanoseries (Nano ZS, Malvern Instruments, UK). SAXS was used to analyze the prepared MSNnanoformulations using XPERT PRO – PANalytical – Netherland. The target is a CuK_{α} producing X-rays at a wavelength of $\lambda = 1.54$ Å. All powder samples were analyzed at angle 2θ, ranging from 0.1°to 5°(scattering vector (q) ranges from 0.007 to 0.355 1/Å) where $q = (4\pi \sin \theta / \lambda)$ with a step size $2\theta = 0.0°$ at a temperature of 25 °C. WAXS of all MSNs was measured using the same X-ray diffractometer that was used to measure SAXS and LAXS. All powder samples were analyzed at angle 2θ, ranging from 10° to 80° with a step size of $2\theta = 0.02°$ at a temperature of 25 °C.

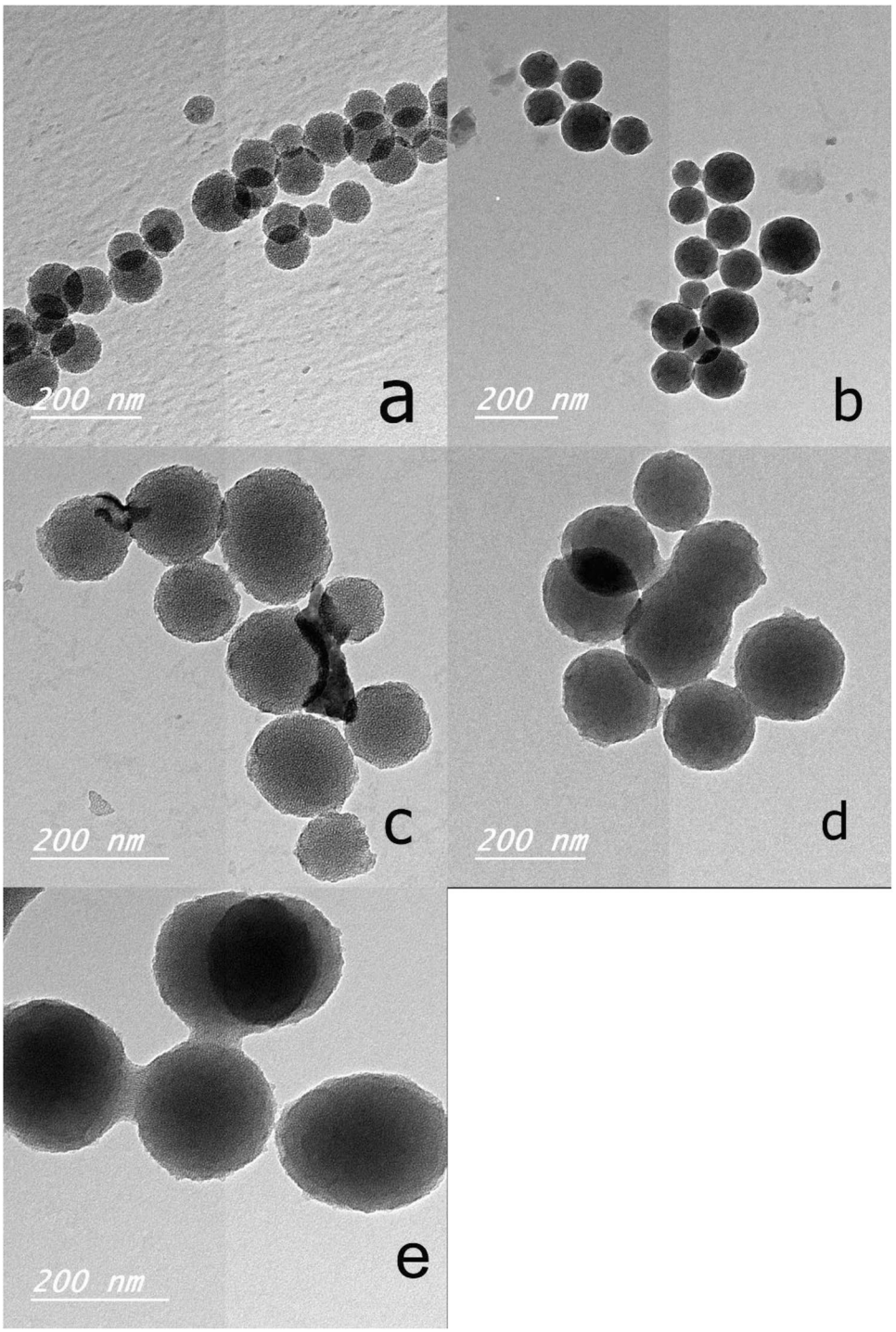

Fig. 1 TEM images for the prepared MSN1, MSN2, MSN3, MSN4 and MSN5 samples with different concentrations of NH_4OH, (**a**): 0.7, (**b**): 1.4, (**c**): 2.4, (**d**): 4.2 and (**e**): 5.6 mg/ml, respectively

Nitrogenadsorption/desorption isotherms (N_2-isotherm) of the prepared MSN samples were obtained using Quantachrome Nova Win–Data Acquisition and Reduction for NOVA instruments ©1994–2016, Quantachrome Instruments (version 11.04). The MSNs were degassed at − 200 °C before measurements. The specific surface area of the MSNs was determined using Brunauer–Emmett–Teller (BET) method. Barrett–Joyner–Halenda (BJH) method was used for pore analysis. AFM was used to examine the samples' surface properties (roughness) in a noncontact mode using Wet–SPM9600 (scanning probe microscope) (Shimadzu, Japan). The area of the resultant scanning images was 5 µm × 5 µm and obtained scanning rate was 0.8 Hz/s.

2.4 In Vitro Drug Release

2.4.1 Loading of DOX on MSNs

The samples (40 g each) (MSN1, MSN2, MSN3, MSN4, and MSN5) were dissolved in 3-ml deionized water, and then 1-ml DOX (2 mg/ml) was added. The suspensions were left in a bath shaker for 24 h at 37 °C and 100 rpm. After 24 h, the suspensions were centrifuged at 5000 rpm for 0.5 h. The encapsulation efficiency (EE) was determined using the formula below:

$$\text{EE } \% = \frac{\text{Initial concentration of DOX} - \text{Concentration of DOX in supernatant}}{\text{Initial concentration of DOX}} \times 100$$

2.4.2 Release of DOX from MSNs

In vitro drug release of DOX from MSNs was assessed. For all MSN samples, the pellet produced by centrifugation in the DOX loading step was resuspended in 5-ml PBS pH 7.4. The suspension was transferred into a dialysis bag suspended in 20-ml PBS in closed tubes. Finally, the tubes were shaken for 48 h at 37 °C. The cumulative release of DOX from MSN samples was determined as the concentration of the released DOX divided by the concentration of DOX in the nanoparticles.

$$\text{Cumulative release } \% = \frac{\text{Concentration of DOX released}}{\text{Concentration of DOX in the nanoparticles}} \times 100$$

3 Results and Discussion

3.1 MSN Characterization Using TEM

TEM images (Fig. 1a, b, c, & d) demonstrated that the MSN1, MSN2, MSN3, and MSN4 samples, respectively, were composed of spherical nanoparticles [49], whereas the MSN5 sample (Fig. 1e) was oval. The mean sizes increased

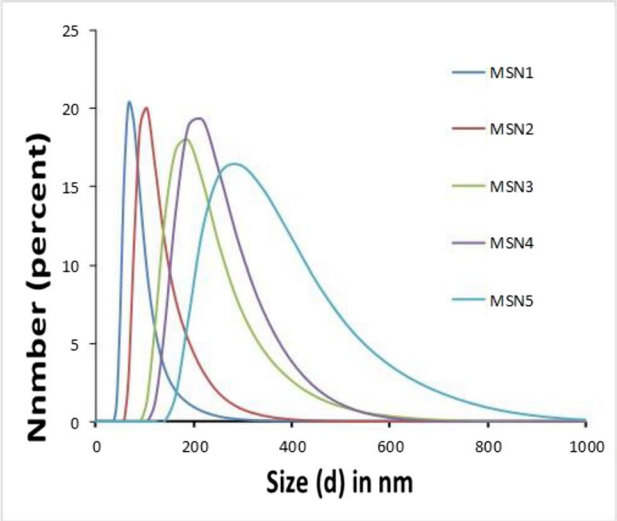

Fig. 2 Particle size distribution of MSN1, MSN2, MSN3, MSN4 and MSN5 samples

with increasing concentration of NH_4OH (pH increased), 64.18 ± 6.8, 90.46 ± 7.1, 118.98 ± 7.01, 152.7 ± 1.7, and 173.9 ± 9.36 nm for MSN1, MSN2, MSN3, MSN4, and MSN5 samples, respectively. The enlargement of the hydrophobic core of template CTAB as the protonation degree of the synthesis solutions decreased (increasing the pH) increased the size of MSNs [49]. The images showed well-dispersed nanoparticles for MSN1, MSN2, and MSN3 samples (Fig. 1a, b, & c). However, MSN4 and MSN5 samples (Fig. 1d and e) showed an increase in the aggregation of

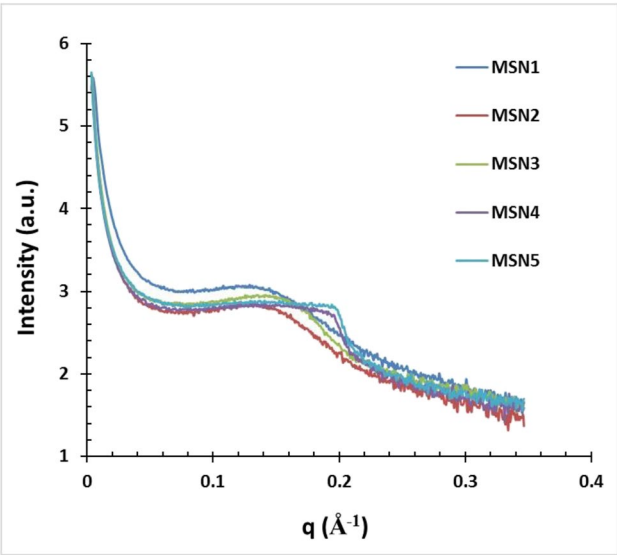

Fig. 3 SAXS profiles for all samples of mesoporous silica nanoparticles (MSN1, MSN2, MSN3, MSN4 and MSN5)

MSNs due to the increased pH. The latter resulted in a strong electrostatic interaction between silica and cationic surfactant (CTAB), as well as fast silica condensation rate and fast assembling and growth of silica with surfactant [50].

3.2 MSN Characterization Using DLS

Dynamic light scattering assessment showed an increase in the average hydrodynamic size of MSNs with increasing NH_4OH, from 0.7 to 5.6 mg/ml (with increased pH) (Fig. 2). The sizesof the nanoparticles were 85.07 ± 16, 124.3 ± 23.4, 215.4 ± 41.8, 239 ± 39.2, and 339.9 ± 63 nm for MSN1, MSN2, MSN3, MSN4, and MSN5, respectively. The increase in the size of MSNs obtained using the DLS technique compared to that obtained using the TEM could be attributed to the inclusion of the hydration layer formed around the nanoparticles when presented in a medium [51, 52].

This study revealed moderate stability of the synthesized MSNs; ZPs were -27.1, -23.8, -23.6, -28.6, and -29.4 mV for MSN1, MSN2, MSN3, MSN4, and MSN5, respectively. The results showed that the ZP for MSN1, MSN2, and MSN3 samples decreases as the size of nanoparticles increases. However, for MSN4 and MSN5, the increase in the ZP value compared to all other samples was due to aggregation, as shown in TEM images (Fig. 1d and e). The distribution of the silanol group on the surface of MSNs made their surfaces negatively charged [53, 54]. The variation in the values of the ZP is due to the distribution and concentration variations of silanol groups on the surface of the MSNs [55].

3.3 X-ray Scattering Characterization

SAXS measurements were performed for all samples. The scattering profiles were recorded at a scattering angle (2θ) ranging from 0.1° to 5.0°. Measured SAXS profiles (scattering intensity versus scattering vector, q) for all prepared samples are shown in Fig. 3. The scattering profiles for MSN1, MSN2, and MSN3 were similar; however, there was an observed shift in the shoulder at large values of scattering vector (from 0.15 to 0.22 $Å^{-1}$) for MSN4 and MSN5 samples, respectively. This shift in the shoulder position could be attributed to the corresponding change in shape (turning slightly oval) and aggregation of nanoparticles as disclosed in the TEM (Fig. 1d and e). The presence of oscillations at high q values (from 0.2 to 0.355 $Å^{-1}$) in all samples was due to the spherical shape of nanoparticles. Moreover, it indicated a degree of monodispersity [56].

WAXS was performed for all samples. The WAXS spectra of samples were plotted (Fig. 4) and showed one characteristic peak at approximately $2\theta = 22.5°$. WAXS profiles of the investigated samples showed no detectable differences. WAXS could not detect the changes in the internal molecular structure of prepared MSNs.

3.4 Gas Isotherm (N_2-Isotherm) of MSNs

Nitrogen adsorption/desorption on the surface of the nanoparticles were performed to obtain the pore volume and specific surface area of MSNs from the analysis of the isotherm of each sample. Figure 5 shows the isotherm plots for samples MSN1, MSN2, MSN3, MSN4, and MSN5.

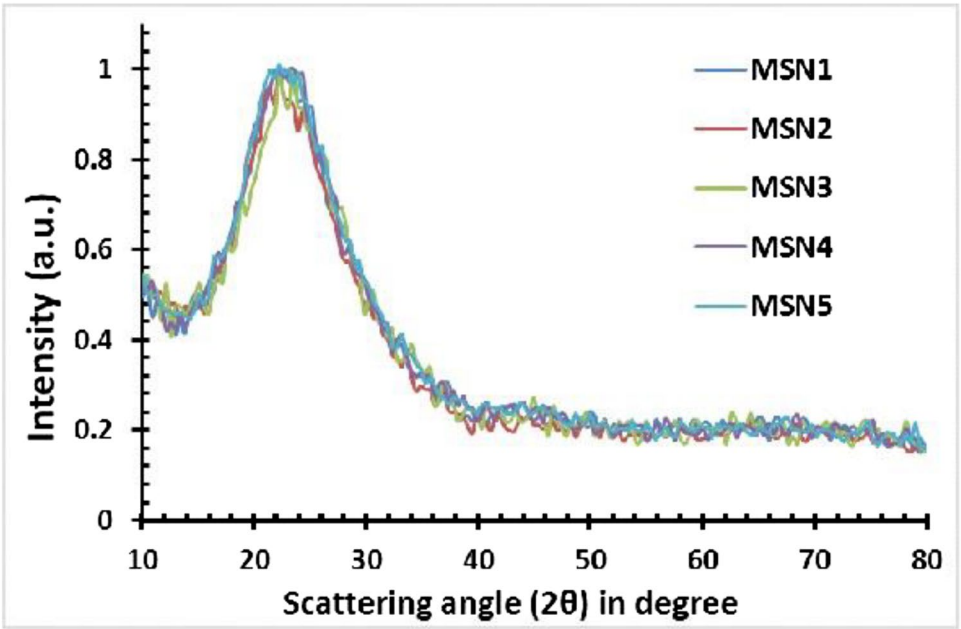

Fig. 4 WAXS spectra for MSN1, MSN2, MSN3, MSN4 and MSN5 samples

From the figure, the type of isotherm is IV isotherm for the investigated samples, regardless of increasing in size. The IV isotherm appeared due to the mesoporous nature of the nanoparticles [57, 58].

The specific surface areas obtained using Brunauer–Emmett–Teller (BET) method for isotherm showed fluctuation in values. This could be due to the aggregation discussed earlier in the TEM image (Fig. 1) [7]. By the Barrett–Joyner–Halenda (BJH) method, the pore volume is derived from the adsorption branch of isotherms of MSN samples. The volume of pores was found to be 0.897, 0.356, 0.243, 0.180, and 0.142 (cc/g) for MSN1, MSN2, MSN3, MSN4, and MSN5, respectively. The pore volume of nanoparticles decreased with size.

3.5 Roughness of Prepared MSNs Using AFM

AFM was conducted to investigate the surface topography of all MSN samples. The 3D images of the surfaces of nanoparticles are shown in Fig. 6a, b, c, d, and e for samples MSN1, MSN2, MSN3, MSN4, and MSN5, respectively. The surface roughness were 2.29 ± 0.993, 1.69 ± 0.448, 1.66 ± 0.471, 1.524 ± 0.43, and 1.79 ± 0.618 µm, respectively. For samples MSN1, MSN2, MSN3, and MSN4, as the size of MSNs increased, the roughness of nanoparticle surfaces decreased, except in sample MSN5, where the roughness increased. The increase in roughness for sample MSN5 can be attributed to the aggregation found in MSN5, as illustrated in the TEM image (Fig. 1e).

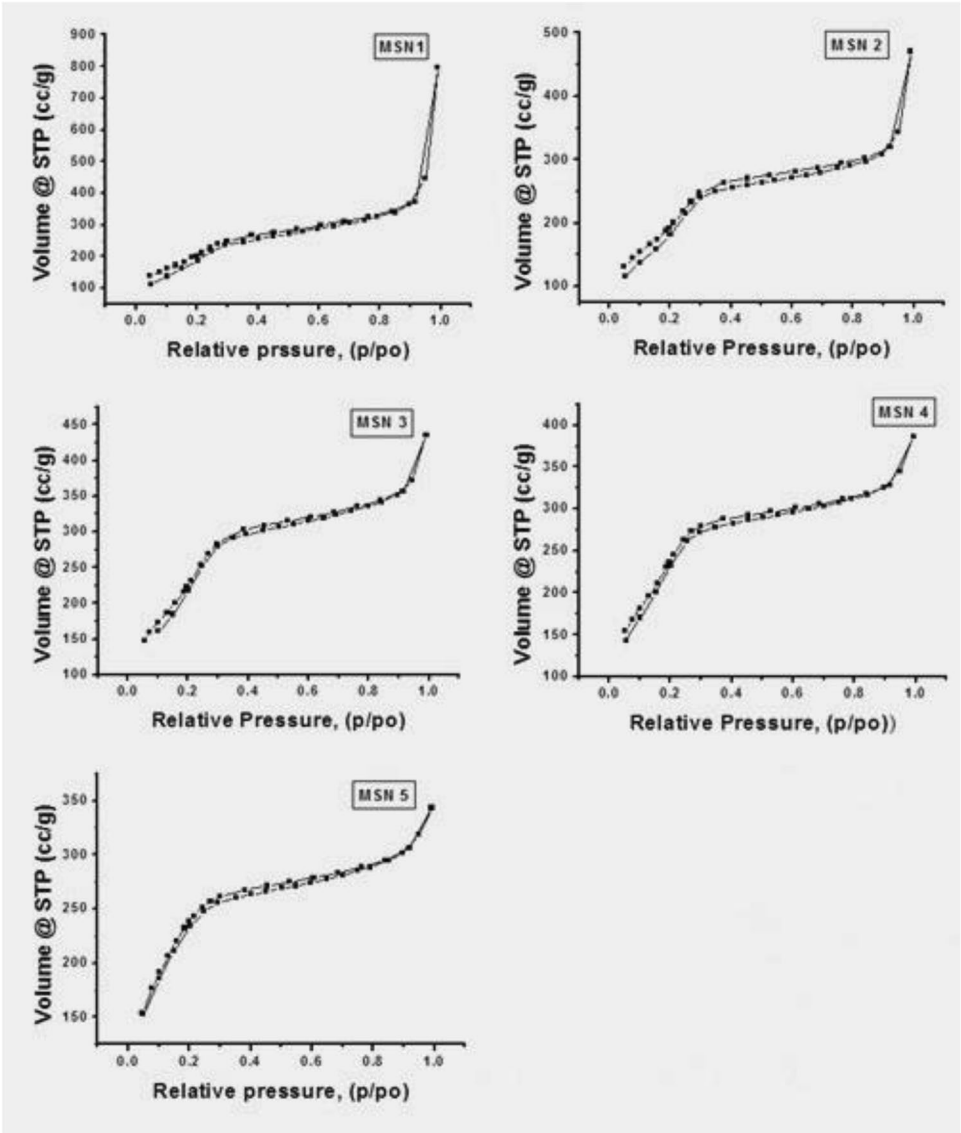

Fig. 5 Nitrogen adsorption / desorption isotherm for MSN1, MSN2, MSN3, MSN4 and MSN5 samples

3.6 Loading of DOX on MSNs

The encapsulation efficiency (EE) of DOX into the investigated MSNs was determined. As the size of nanoparticles increased, the loading efficiency decreased. EEs were 92.2%, 82.8%, 72.2%, 72.1%, and 71.9% for MSN1, MSN2, MSN3, MSN4, and MSN5, respectively. This is due to a decrease in the pore volume of nanoparticles as the size increased (like the data previously produced using the N_2-isotherm). For samples MSN3, MSN4, and MSN5, the EEs are the same as their nanoparticles had comparable pore volumes.

3.7 Release of DOX from MSNs

The synthesized nanoparticles were loaded using DOX to optimize the best preparation conditions for drug delivery applications. The cumulative drug release for all samples is shown in Fig. 7. Sample MSN5 (with size 173.9 ± 9.36 nm, pore volume 0.142 cc/g, roughness 1.79 µm, and smallest EE, 71.9%) showed the highest drug release. This implied that it would not be preferred for drugdelivery applications because drugs cannot be stored in its pores for a long time. Therefore, the drug might be released into the biological system before reaching the target cell.

However, the MSN1 sample (with the largest pore volume 0.897 cc/g, roughness 2.29, EE 92.2%, and smallest size 64 ± 6.8 nm) showed the lowest drug release profile at the assigned time intervals. This indicated that the MSN1 sample released the drug in minimal amounts despite its high EE. The low rate of drug release seemed to be due to the association of the drug and tiny silica pores of MSN1. These features would be favorable, except that the release

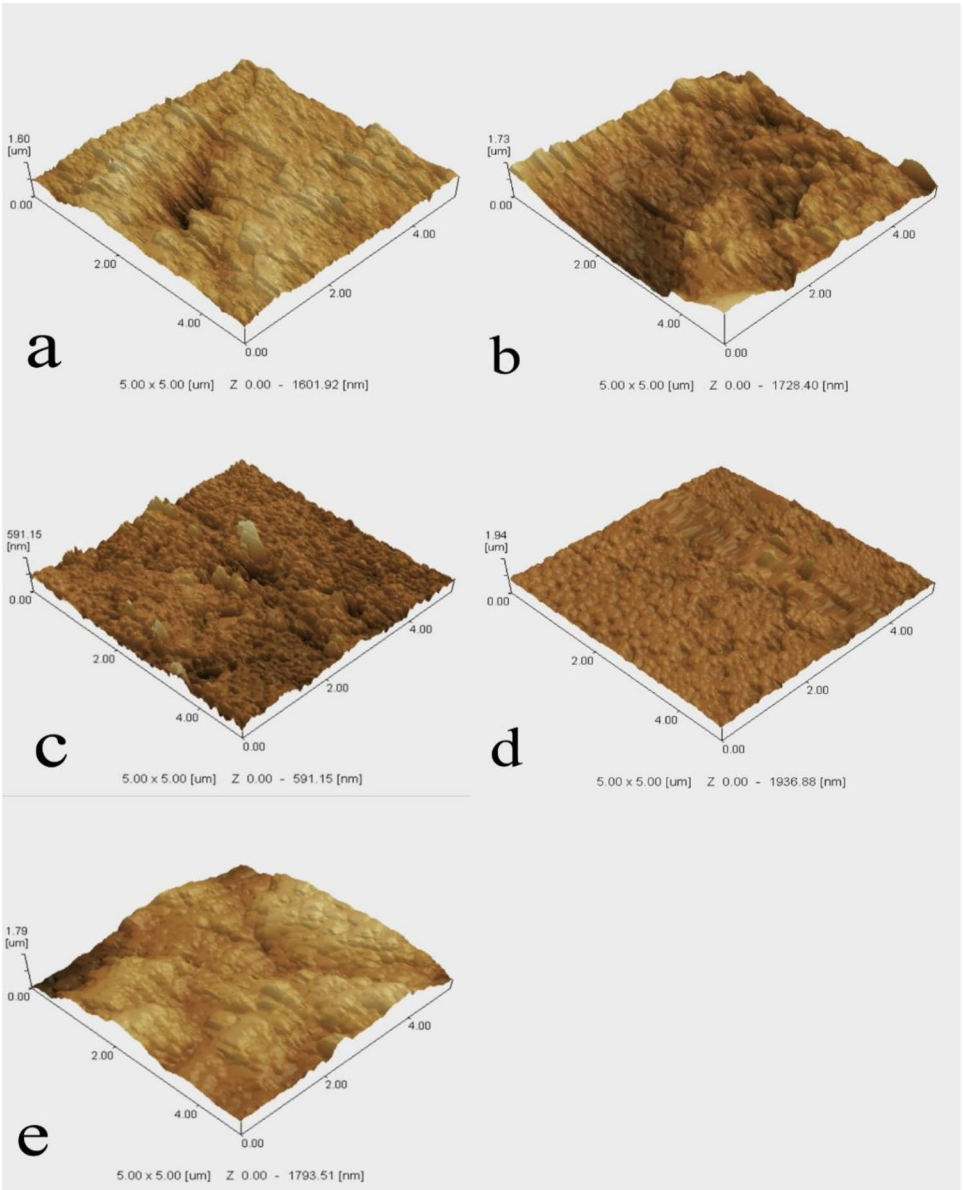

Fig. 6 AFM analysis showing surface roughness 3D image of samples (**a**) MSN1, (**b**) MSN2, (**c**) MSN3, (d) MSN4 and (**e**) MSN5 with field5 µm × 5 µm

rate might be insufficient for efficient drug delivery. However, samples MSN2, MSN3, and MSN4 represented a compromise between the high encapsulation and release as in MSN5 and the low encapsulation and release as in MSN1. A choice of these three MSNs for drug delivery purposes would be reliable.

The important characteristic for enhancing drug delivery to target cells is the size of MSNs. The particle size affects the cellular uptake of MSNs as it affects the interaction between MSNs and the cell membrane [17–20]. When the sizes of nanoparticles are greater than 100 nm each and aggregated, toxicity may increase [29, 59] and cause fast uptake of the reticuloendothelial system (RES) [32, 60, 61]. Therefore, samples MSN3, MSN4, and MSM5 would not be preferred for drug delivery applications because their particle size was more significant than 100 nm (118.98 ± 7.01, 152.7 ± 1.7, and 173.9 ± 9.36 nm, respectively). Moreover, aggregation was reported for MSN4 and MSN5, as shown in TEM images (Fig. 1d and e).

Small-sized nanoparticles have advantages as nanocarriers for drug delivery applications due to their ability to overcome biological system barriers, showing significant uptake by target cells and biocompatibility [5, 62–64]. MSNs less than 100 nm would be the best choice of the investigated formulations as carriers of drugs in drug delivery systems. MSN1 sample with small size (64.18 ± 6.8 nm), large pore volume (0.89 cc/g), and high EE (92.2%) is the best choice for biological applications. MSN2 sample with a small size (90.46 ± 7.1 nm), large pore volume (0.356 cc/g), and high EE (82.8%) is another choice for biological applications. According to the application, MSN1 or MSN2 samples can be used. If an application needs a high drug release rate, MSN2 is the best choice. However, MSN1 is used when the application requires a low drug release rate. The large pore volume has the advantage of easy biodegradation as the thickness of the silica wall becomes thinner with increased pore volume [7, 65].

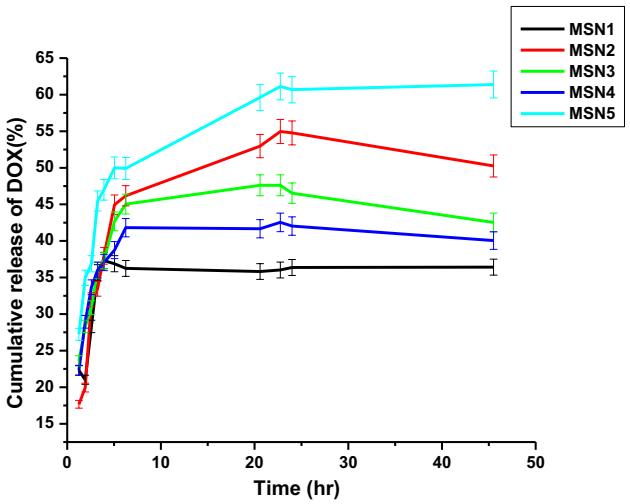

Fig. 7 Cumulative release of DOX from prepared MSNs samples. The error bars are calculated for three different experiments

4 Conclusions

The study of MSNs for drug nanocarriers in drug delivery applications was achieved by preparing different formulations of MSNs. MSN samples were synthesized by varying the concentration of ammonium hydroxide as a catalyst while keeping all other synthetic conditions constant. These MSNs were characterized using different techniques. The preparation of MSNs with different properties (size, porevolume, roughness, and zeta potential) was feasible. It would probably affect their capability as nanocarriers and would allow the use of MSNs in different biological and medical applications. All MSN samples exhibited a high EE of DOX. The drug release profile for all helped determine the best formulation for drug delivery applications. Considering all investigated parameters, we found that the best formulations for drug delivery applications are the MSN1 and MSN2 samples.

Author Contribution Mohamed M. Fathy, Wael M Elshemey and Heba Mohamed Fahmy conceived of the presented idea. Fatma M Yassin, Mohamed M. Fathy and Heba Mohamed Fahmy conceived and planned the experiments. Fatma M Yassin, Mohamed M. Fathy and Heba Mohamed Fahmy carried out the experiments. Fatma M Yassin contributed to samples characterizations. Fatma M Yassin, Wael M Elshemey, Heba Mohamed Fahmy and Mohamed Mahmoud Fathy contributed to the interpretation of the results. All authors contributed to the final version of the manuscript. All authors read and approved the manuscript and all data were generated in-house and that no paper mill was used.

Funding Open access funding provided by The Science, Technology & Innovation Funding Authority (STDF) in cooperation with The Egyptian Knowledge Bank (EKB).

Data Availability All data generated or analyzed during this study are included in this published article (the raw data will be available in case required them from the authors).

Declarations

Competing Interests The authors declare that they have no known competing financial interests or personal relationships that could have appeared to influence the work reported in this paper.

Consent to Participate Informed consent was obtained from all individual participants included in the study.

Consent for Publication All authors agreed to publish this study at the silicon journal.

Conflict of Interest The authors have no conflicts of interest to declare that are relevant to the content of this article.

Research Involving Human Participants and/or Animals This study were not included neither animals nor human.

References

1. Samir A, Elgamal BM, Gabr H, Sabaawy HE (2015) Nanotechnology applications in hematological malignancies. Oncol Rep 34(3):1097–1105
2. dos Santos SN, Dos Reis SRR, Pires LP, Helal-Neto E, Sancenón F, Barja-Fidalgo TC, Santos-Oliveira R (2017) Avoiding the mononuclear phagocyte system using human albumin for mesoporous silica nanoparticle system. Microporous Mesoporous Mater 251:181–189
3. McMillan J, Batrakova E, Gendelman HE (2011) Chap. 14. Cell delivery of therapeutic nanoparticles. In: Progress in Molecular Biology and Translational Science 104, 563–601. Academic, Cambridge
4. Vallet-Regí M, Colilla M, Izquierdo-Barba I, Manzano M (2018) Mesoporous silica nanoparticles for drug delivery: current insights. Molecules 23(1):47
5. Skibińska M, Pikus S (2017) Small-angle X-ray scattering (SAXS) studies of the structure of mesoporous silicas. Nucl Instrum Methods Phys Res Sect B 411:72–77
6. Kent N, Nigra MM, Coppens MO (2017) Effect of stirring rate on the morphology of FDU-12 mesoporous silica particles. Microporous Mesoporous Mater 249:61–66
7. Marin R, Freris I, Marchiori M, Moretti E, Storaro L, Canton P, Lausi A, Benedetti A, Riello P (2014) Mesoporous silica nanoparticles with tunable pore size for tailored gold nanoparticles. J Nanopart Res 16:2245
8. Lee N, Kim T, Kim J, Hyeon T (2011) Multifunctional mesoporous silica nanocomposite nanoparticles for theranostic applications. Acc Chem Res 44:893–902
9. Martín-Saavedra E, Ruíz-Hernández A, Boré D, Arcos M, Vallet-Regí N, Vilaboa, (2010) Magnetic mesoporous silica spheres for hyperthermia therapy. Acta Biomater 6(12):4522–4531
10. Ji Q, Mori T, Naito M, Yamauchi Y, Abe H (2013) Hill, Enzyme nanoarchitectonics: organization and device application. Chem Soc Rev 42:6322–6345
11. Slowing II, Trewyn BG, Giri S, Lin VY (2007) Mesoporous silica nanoparticles for drug delivery and biosensing applications. Adv Funct Mater 17(8):1225–1236
12. Egodawatte S, Kaplan DI, Larsen SC, Serkiz SM, Seaman JC (2016) Functionalized magnetic mesoporous silica nanoparticles for U removal from low and high pH groundwater. J Hazard Mater 317:494–502
13. Mizoshita N, Tanaka H (2017) Interface-assisted synthesis of mesoporous silica nanoparticles using neat tetraalkoxysilanes. Microporous Mesoporous Mater 239:1–8
14. Vivero-Escoto J, Slowing II, Garrone E, Onida B, Lin VSY (2009) Cell-induced intracellular controlled release of membrane impermeable cysteine from a mesoporous silica nanoparticle-based drug delivery system. Chem Commun 22:3219–3221
15. Kim S, Park C, Lee H, Park HJ, Kim C (2010) Glutathione-induced intracellular release of guests from mesoporous silica nanocontainers with cyclodextrin gatekeepers. Adv Mater 22:4280–4283
16. Kulanthaivel S, Mondal A, Mishra S, Banerjee B, Bhaumik A, Giri S (2017) Mesoporous silica nanoparticle based enzyme responsive system for colon specific drug delivery through guar gum capping. Colloids Surf B 150:352–361
17. Cote MF, -Gaudreault RC, Fortin MA, Kleitz F (2016) Size-controlled functionalized mesoporous silica nanoparticles for tunable drug release and enhanced anti-tumoral activity. Chem Mater 28:4243–4258
18. Cendrowski K, Barylak M, Roginska D, Tarnowski M, Tkacz M, Kurzawski M, Machalinski B, Mijowska E, Drozdzik M (2015) Study on size effect of the silica nanospheres with solid core and mesoporous shell on cellular uptake. Biomed Mater 10:065012
19. Nienhaus K, Nienhaus GU (2014) Engineered nanoparticles interacting with cells: size matters. J Nanobiotechnol 12:5
20. Gabrielsson S, Strømme M, Scheynius A, Garcia-Bennett AE (2007) Mesoporous silica particles induce size dependent effects on human dendritic cells. Nano Lett 7:3576–3582
21. Labhasetwar V, Walter E, Levy RJ, Amidon GL (1997) The mechanism of uptake of biodegradable microparticles in Caco-2 cells is size dependent. Pharm Res 14:1568–1573
22. Sahar MR, Ghoshal SK, Arifin R, Rohani MS, Hamzah K, Jandra M (2013) Natural Fe3O4 nanoparticles embedded zinc–tellurite glasses: Polarizability and optical properties. Mater Chem Phys 138:174–178
23. Tong L, Ren X, Li Q, Ding H, Yang H (2013) Bifunctional Fe3O4@ C/YVO4: Sm3 + composites with the core–shell structure. Mater Chem Phys 139:73–78
24. Yanagisawa T, Shimizu T, Kuroda K, Kato C (1990) The preparation of alkyltriinethylaininonium–kaneinite complexes and their conversion to microporous materials. Bull Chem Soc Jpn 63(4):988–992
25. Kresge CT, Leonowicz ME, Roth WJ, Vartuli JC, Beck JS (1992) Ordered mesoporous molecular sieves synthesized by a liquid-crystal template mechanism. Nature 359(6397):710
26. Burkett SL, Davis SA, Fowler CE, Mendelson NH, Sims SD, Walsh D (1997) Whilton. Sol – gel synthesis of organized matter. Chem Mater 9:2300–2310
27. Hoffmann F, Cornelius M, Morell J, Fröba M (2006) Silica-based mesoporous organic–inorganic hybrid materials. Angew Chem Int Ed 45(20):3216–3251
28. Huang Q, Li C, Bao C, Liu Z, Li F, Zhu L (2010) Anticancer drug release from a mesoporous silica based nanophotocage regulated by either a one-or two-photon process. J Am Chem Soc 132:10645–10647
29. Lin CL, Haynes (2010) Impacts of mesoporous silica nanoparticle size, pore ordering, and pore integrity on hemolytic activity. J Am Chem Soc 132:4834–4842
30. Asaro F, Benedetti A, Freris I, Riello P, Savko N (2010) Evolution of the nonionic inverse microemulsion – acid – TEOS system during the synthesis of nanosized silica via the sol – gel process. Langmuir 26(15):12917–12925
31. Argyo C, Bein T (2010) Impact of different PEGylation patterns on the long-term bio-stability of colloidal mesoporous silica nanoparticles. J Mater Chem 20:8693–8699

32. Shi J (2011) Mesoporous silica nanoparticle based nano drug delivery systems: synthesis, controlled drug release and delivery. pharmacokinetics and biocompatibility. J Mater Chem 21:5845–5855
33. Wang JG, Sun PC, Ding DT, Chen TH (2009) Effect of alcohol on morphology and mesostructure control of anionic-surfactant-templated mesoporous silica (AMS). J Colloid Interface Sci 331:156–162
34. Han BH, Yang Y (2004) Simple synthesis route to monodispersed SBA-15 silica rods. J Am Chem Soc 126:14348–14349
35. Fan J, Tian B, Zhao D (2004) Morphology development of mesoporous materials: a colloidal phase separation mechanism. Chem Mater 16:889–898
36. Hwang YK, Chang JS, Kwon YU, Park SE (2004) Microwave synthesis of cubic mesoporous silica SBA-16. Microporous Mesoporous Mater 68(1–3):21–27
37. Dos Reis TVS, Cosentino IC, Fantini MCDA, Matos JR, Bruns RE (2010) Factorial design to optimize microwave-assisted synthesis of FDU-1 silica with a new triblock copolymer. Microporous Mesoporous Mater 133:1–9
38. Yan X, Kruk M (2010) Synthesis of ultralarge-pore FDU-12 silica with face-centered cubic structure. Langmuir 26:14871–14878
39. Kruk M (2015) Versatile surfactant/swelling-agent template for synthesis of large-pore ordered mesoporous silicas and related hollow nanoparticles. Chem Mater 27:679–689
40. Nooney RI, Thirunavukkarasu D, Chen Y, Josephs R, Ostafin AE (2002) Synthesis of nanoscale mesoporous silica spheres with controlled particle size. Chem Mater 14(11):4721–4728
41. Vazquez NI, Gonzalez Z, Ferrari B, Castro Y (2017) Synthesis of mesoporous silica nanoparticles by sol–gel as nanocontainer for future drug delivery applications. Bol Soc Esp Cerám Vidr 56(3):139–145
42. Guo X, Gao K, Gutsche A, Seipenbusch M, Nirschl H (2015) Combined small-and wide-angle X-ray scattering studies on oxide-supported Pt nanoparticles prepared by a CVS and CVD process. Powder Technol 272:23–33
43. Akiba I, Harrisson S, Wooley KL (2008) Facile formation of uniform shell-crosslinked nanoparticles with built-in functionalities from N-hydroxysuccinimide-activated amphiphilic block copolymers. Adv Funct Mater 18:551–559
44. Rao SN, Fitzmaurice D (2000) Characterization of protein aggregated gold nanocrystals. J Phys Chem B 104:4765–4776
45. Lin JS, Lam YF, Hu MC, Schaefer DW, Harris MT (2003) Size, volume fraction, and nucleation of Stober silica nanoparticles. J Colloid Interface Sci 266:346–358
46. Shaw S, Benning LG (2009) Quantification of initial steps of nucleation and growth of silica nanoparticles: An in-situ SAXS and DLS study. Geochim Cosmochim Acta 73(18):5377–5393
47. Feichtenschlager B, Kickelbick G, Peterlik H (2012) Effect of interparticle interactions on size determination of zirconia and silica based systems–A comparison of SAXS, DLS, BET, XRD and TEM. Chem Phys Lett 521:91–97
48. Chen H, He J, Tang H, Yan C (2008) Porous silica nanocapsules and nanospheres: dynamic self-assembly synthesis and application in controlled release. Chem Mater 20(18):5894–5900
49. Deodhar GV, Adams ML, Trewyn BG (2017) Controlled release and intracellular protein delivery from mesoporous silica nanoparticles. Biotechnol J 12(11):600408
50. Mou CY, Lin HP (2013) Synthesis of mesoporous silica nanoparticles. Chem Soc Rev 42:3862–3875
51. Cui Y, Dong H, Cai X, Wang D, Li Y (2012) Mesoporous silica nanoparticles capped with disulfide-linked PEG gatekeepers for glutathione-mediated controlled release. ACS Appl Mater Interfaces 4(6):3177–3183
52. Zhang Z, Mayoral A, Melián-Cabrera I (2016) Protocol optimization for the mild detemplation of mesoporous silica nanoparticles resulting in enhanced texture and colloidal stability. Microporous Mesoporous Mater 220:110–119
53. Lvov Y, Ariga K, Onda M, Ichinose I, Kunitake T (1997) Alternate assembly of ordered multilayers of SiO2 and other nanoparticles and polyions. Langmuir 13(23):6195–6203
54. Zhang Y, Wang J, Bai X, Jiang T, Zhang Q, Wang S (2012) Mesoporous silica nanoparticles for increasing the oral bioavailability and permeation of poorly water soluble drugs. Mol Pharm 9(3):505–513
55. Zhuravlev LT (2000) The surface chemistry of amorphous silica Zhuravlev model. Colloids Surf A: Physicochem Eng Asp 73(1–3):1–38
56. Bertholdo R, dos Reis FV, Pulcinelli SH, Santilli CV (2010) SAXS study of monodispersed silica nanospheres obtained by an amino acid route. J Non-Cryst Solids 356(44–49):2622–2625
57. Al-Attar L, Dyer A, Harjula R (2003) Uptake of radionuclides on microporous and layered ion exchange materials. J Mater Chem 13(12):2963–2968
58. Bore MT, Rathod SB, Ward TL, Datye AK (2003) Hexagonal mesostructure in powders produced by evaporation-induced self-assembly of aerosols from aqueous tetraethoxysilane solutions. Langmuir 19(2):256–264
59. Yu T, Malugin A, Ghandehari H (2011) Impact of silica nanoparticle design on cellular toxicity and hemolytic activity. ACS Nano 5(7):5717–5728
60. Wu SH, Lin YS, Hung Y, Chou YH, Hsu YH, Chang C, Mou CY (2008) Multifunctional mesoporous silica nanoparticles for intracellular labeling and animal magnetic resonance imaging studies. ChemBioChem 9(1):53–57
61. Huang X, Li L, Liu T, Hao N, Liu H, Chen D, Tang F (2011) The shape effect of mesoporous silica nanoparticles on biodistribution, clearance, and biocompatibility in viv. ACS Nano 5(7):5390–5399
62. Prokop A, Davidson JM (2008) Nanovehicular intracellular delivery systems. J Pharm Sci 97(9):3518–3590
63. Vivero-Escoto JL, Slowing II, Trewyn BG, Lin VSY (2010) Mesoporous silica nanoparticles for intracellular controlled drug delivery. Small 6(18):1952–1967
64. Biswas AK, Islam MR, Choudhury ZS, Mostafa A, Kadir MF (2014) Nanotechnology based approaches in cancer therapeutics. Adv Nat Sci: Nanosci Nanotechnol 5(4):043001
65. Patel KD, Leong KW, Kim HW (2017) Progress in nanotheranostics based on mesoporous silica nanomaterial platforms. ACS Appl Mater Interfaces 9:10309–10337